Journal of Catalysis **205,** 67–85 (2002)
doi:10.1006/jcat.2001.3419, available online at http://www.idealibrary.com on IDEAL®

Reaction Kinetics Study and Analysis of Reaction Schemes for Isobutane Conversion over USY Zeolite

Marco A. Sanchez-Castillo,* Nitin Agarwal,* Christian Miller,* Randy D. Cortright,* Rostam J. Madon,† and J. A. Dumesic*,[1]

*Department of Chemical Engineering, University of Wisconsin, Madison, Wisconsin 53706; and †Engelhard Corporation, 101 Wood Avenue, Iselin, New Jersey 08830

Received April 16, 2001; revised September 17, 2001; accepted September 17, 2001

Reaction kinetics studies were conducted for isobutane conversion over a USY zeolite catalyst at a total pressure of 1 atm and for temperatures of 523 and 573 K. The catalyst is inactive for isobutane conversion in the absence of feed olefins at these temperatures; however, a stable catalyst performance was achieved for levels of isobutylene in the feed ranging from approximately 50 to 400 ppm. The rates of production of *n*-butane, propane, isopentane, propylene, 1-butylene, *cis*-2-butylene, and *trans*-2-butylene were measured for the aforementioned temperatures and isobutylene feed concentrations at isobutane inlet concentrations of 20 and 80%. A kinetic model for isobutane conversion over USY zeolite was developed based on the following families of reactions: adsorption/desorption steps, oligomerization/β-scission processes, isomerization steps, hydride transfer processes, and initiation steps. This kinetic model describes the reaction kinetics data collected in the present study of isobutane conversion at low temperatures, and it also describes reaction kinetics data collected at higher temperatures (733–773 K) over a USY zeolite catalyst, where the reaction was initiated by the activation of isobutane.

Key Words: **isobutane; USY zeolite; reaction kinetics studies.**

INTRODUCTION

Solid acid catalysts are used widely in the chemical and petrochemical industries for hydrocarbon conversion processes. For example, acidic zeolite-based catalysts are used in fluid catalytic cracking processes, and acid sites are used in combination with metal sites for the bifunctional isomerization of alkanes. Characterization studies of acid sites have been valuable for providing fundamental knowledge about these sites, which are usually probed with basic molecules (e.g., 1–11). Similarly, reaction studies using model compounds have helped to elucidate reaction mechanisms and surface chemistry on acid sites (10, 12–34). However, the challenge still remains to quantitatively relate the nature of acid sites to their catalytic performance. The critical need in this respect is to devise a rigorous yet convenient model that can fundamentally quantify the catalytic properties of acid sites in terms of intrinsic parameters, such as rate constants and activation energies of reaction steps, preferably elementary steps, instead of only in terms of overall catalytic activity and selectivity. Difficulties arise when estimating rate constants and activation energies for reactions of hydrocarbons over solid acid catalysts due to (i) catalyst deactivation with time on stream via coke formation, (ii) the presence of a large number of reaction steps and products, and (iii) the fact that these steps give rise to multiple yet connected catalytic cycles. Moreover, the temperature range over which reaction measurements may be conveniently conducted is often narrow (e.g., 100 K), thus leading to uncertainties when estimating activation energies and pre-exponential factors caused by the difficulty in evaluating accurate slope and intercept values.

It is essential to understand the reactivity of acid sites in various environments, for example, whether they are within different zeolites or are influenced by mono or multivalent cations, such as rare earth cations, in the same zeolite. Again, a quantitative but general model is important for this purpose. To that end, we turn to the relatively simple isobutane reaction, initially used by McVicker *et al.* (35), to probe the reaction chemistry on solid acid catalysts (13, 15, 27, 36–48). Previously, Yaluris *et al.* (42, 43) modeled the reaction kinetics of isobutane conversion over USY zeolite between 733 and 773 K, temperatures at which the reactions were initiated by the activation of isobutane (42). Fogash *et al.* (45, 46), investigating the conversion of isobutane over H-mordenite at a low temperature, 473 K, showed that small levels of isobutylene in the feed were necessary to initiate the conversion of isobutane. In our current work we use the experience from these earlier efforts to develop a comprehensive approach that can quantify reaction rates and kinetic parameters of elementary steps over a wide temperature range.

In this paper, we report reaction kinetics measurements for isobutane conversion over a USY zeolite catalyst at low temperatures (523–573 K), under conditions where

[1] To whom correspondence should be addressed. E-mail: dumesic@engr.wisc.edu.

0021-9517/02 $35.00

catalyst deactivation is negligible. We then develop a kinetic model for isobutane conversion over USY zeolite using (i) the data from the present study where the reaction is initiated by the addition of isobutylene (e.g., from 50 to 400 ppm) to the reactor feed and (ii) results from reaction measurements collected previously for isobutane conversion at higher temperatures (733–773 K), where the reaction is initiated by the activation of isobutane (42, 43). The model, over the whole temperature range, is described in terms of the following families of reactions: adsorption/desorption, oligomerization/β-scission, isomerization, hydride transfer, and initiation steps. Importantly, while many combinations of reactions from these families of processes are possible, leading to a variety of reaction products, the kinetic model is based on a limited number of kinetic parameters that describe the reactivity trends for different hydrocarbon species. Accordingly, the kinetic model serves to describe an apparently complex product distribution in terms of a limited number of kinetic parameters for various families of reactions. This small set of kinetic parameters then becomes a surrogate for the more complex set of reaction kinetics data, providing a framework to compare quantitatively the performances of different solid acid catalysts. This approach provides information about how various reaction steps in catalytic cycles may be influenced by changes in catalyst properties related, for example, to the environment of the acid sites within different zeolitic structures or by cations exchanged on tetrahedral–oxygen–tetrahedral sites.

EXPERIMENTAL

The ultrastable Y zeolite (USY zeolite) in this study is a component of commercial fluid catalytic cracking catalysts and is used by itself without any matrix or binder components. We measured its Brønsted and Lewis acidity by Fourier transform infrared spectroscopy using pyridine as the probe molecule. Details of the experiments, carried out with a Perkin–Elmer 1750 spectrometer operating in the diffuse reflectance mode using a Spectra Tech controlled-environment cell, are given elsewhere (49). Table 1 gives the acidity values as well as other relevant properties of the catalyst. The table also gives the properties of the FCC catalyst used in the high-temperature work (42). This catalyst consisted of USY in a clay matrix.

Following the procedure described by Fogash *et al.* (45), we carried out kinetics studies using a combination of two quartz flow reactors connected in series. The first reactor, loaded with 0.9 g of a Pt-Sn/L-zeolite catalyst, controls the isobutylene concentration in the feed by varying the dehydrogenation–hydrogenation equilibrium of the isobutane/H_2 gas mixture. This control is done by adjusting the reaction temperature between 473 and 573 K. The feed to the first reactor consisted of different fractions of isobutane (AGA, research grade, 99.99%) hydrogen (Praxair, 99% purity), and helium (Praxair, 99% purity) at a total pressure of 1 atm. Isobutane, used without further purification, had a total hydrocarbon impurity level below 20 ppm. We purified hydrogen via a Deoxo Unit (Engelhard), followed by a molecular sieve bed at 77 K, and helium by passage through an activated molecular sieve bed at 77 K. The total flow rate of feed to the reactor was 60 cm^3 normal temperature and pressure, (NTP)/min. The second reactor was loaded with 0.1 g of a USY zeolite catalyst, and isobutane conversion was studied at 523 and 573 K. Prior to collecting reaction kinetics data, the catalyst was calcined at 773 K for 4 h. We used the same sample of USY zeolite for all kinetics studies. Calcining the catalyst between experiments at 773 K for 4 h in dry O_2 at a flow rate of 160 cm^3(NTP)/min was sufficient to restore its performance for isobutane conversion to that exhibited by a fresh sample.

TABLE 1

Characteristics of the Calcined USY Zeolite Catalysts

	Low-temperature kinetics data	High-temperature kinetics data[a]
Si/Al	4.82	8.3
Rare earth oxide content	<200 ppm	<200 ppm
Total surface area (m^2 g^{-1})	667.8	418
Matrix surface area (m^2 g^{-1})	84.5	144
Zeolite surface area (m^2 g^{-1})	583.3	274
Al_F[b]	32.9	20.6
Unit cell size (Å)	24.546	24.43
Brønsted acid sites (μmol g^{-1})	662	532
Lewis acid sites (μmol g^{-1})	105	304

[a] Yaluris *et al.* (42).
[b] Number of framework Al atoms per unit cell.

Feed compositions to the second reactor consisted of helium, 10% hydrogen, 20 or 80% isobutane, and isobutylene levels nominally equal to 50, 100, 200, 300, and 400 ppm. We collected data sequentially for several reaction conditions. For example, after measuring the rates of isobutane conversion under one set of reaction conditions, we would change the temperature and carry out the next set of measurements. Data collected in such a sequential mode were identical to data collected on freshly regenerated catalysts. We analyzed the products in the effluent gas stream with a gas chromatograph (Hewlett–Packard 5890) equipped with a flame ionization detector (FID) and a 7-ft Alltech column packed with 80/100 mesh 0.19% picric acid on a Graphpac-GC.

RESULTS

Effects of Temperature on Initiation Processes

We initially conducted experiments with the first reactor at 300 K, where the equilibrium for isobutane dehydrogenation is unfavorable. In such a case, with no measurable

isobutylene, and with 20% isobutane and 10% H_2 in the feed, there was no detectable isobutane conversion at temperatures below 600 K. We first detected methane and isobutylene, indicative of isobutane activation, at 623 K, although we obtained measurable rates for *n*-butane, propane, and isopentane formation only at 673 K. These experiments proved that conversion of isobutane over our USY zeolite catalyst may be carried out at temperatures below about 600 K only if isobutylene is fed to the reactor. We also found that with 50 ppm of isobutylene in the feed, we could obtain reproducible and stable rates of isobutane conversion only at temperatures above about 500 K. Accordingly, we settled on a temperature range from 523 to 573 K to carry out the kinetics measurements.

Our conditions are in general agreement with those reported by Fogash *et al.* (46), who did not detect activity for isobutane conversion in the absence of feed olefins on H-mordenite at 473 K. However, Engelhardt reported that an H-mordenite catalyst was active for isobutane conversion at 573 K (44) and also at 473 K (47), even when no olefins were present in the feed. Differences in catalytic properties and acid strength will influence the point of initiation of the isobutane reaction (48); hence, it is necessary to carry out experiments for a given catalyst, as we did, to find the suitable temperature range for experimentation where initiation takes place only via added olefins.

Product Distribution

We observed the following products: propane, *n*-butane, isopentane, propylene, 1-butylene, *trans*-2-butylene, and *cis*-2-butylene, and under certain reaction conditions, traces of 2-methyl-butylenes (less than 5 ppm) and heavier hydrocarbons (e.g., C_6 species) (less than 2 ppm). We did not detect the formation of methane, ethane, and/or aromatics under the conditions of this study.

The main reaction pathways are isomerization to *n*-butane and disproportionation to propane and isopentane. Alkenes are formed via desorption of various adsorbed species, and the corresponding alkanes are formed via hydride transfer between isobutane and the adsorbed species. Other authors have reported similar products for the cracking and isomerization of isobutane over HY or USY zeolites (36–44), HZSM-5 (15, 17, 36, 38), and H-mordenite (20, 44, 45, 47, 50). For comparison with the data of the present study, we note that hydrogen and methane are formed in significant amounts at higher temperatures (42). In addition, measurable amounts of 2-methyl-butenes are also formed at higher temperatures.

Catalyst Stability

Figure 1a shows the rates of production of alkanes as a function of time on stream for isobutane conversion over USY zeolite at 573 K for 80% isobutane, 10% hydrogen, and 400 ppm of isobutylene in the feed. We report rates as turnover frequencies (TOF), where the number of active sites is assumed to be equal to the number of Brønsted acid sites (Table 1). The outlet concentration of isobutylene in the effluent gas and alkane production rates reached steady state after 1 min, and the catalyst performance remained stable with time on stream. Catalyst performance for the production of olefins (i.e., propylene, 1-butylene, *cis*-2-butylene, and *trans*-2-butylene) was also stable with time on stream.

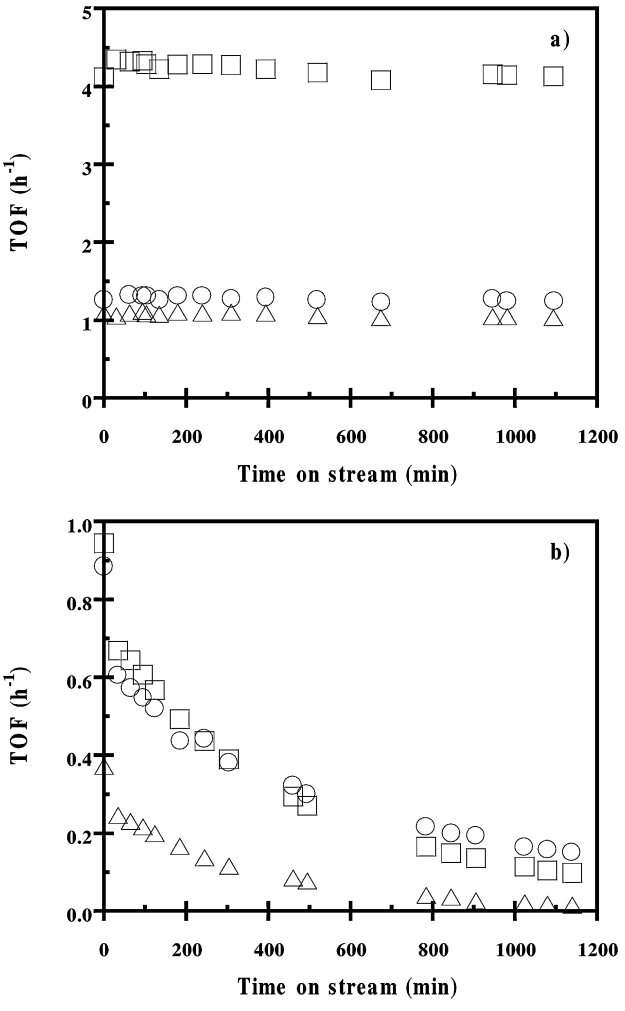

FIG. 1. Paraffin TOF as a function of time on stream. Kinetics studies conducted at (a) 573 K and feed composition = 10% hydrogen, 80% isobutane, and 400 ppm of isobutylene; (b) 523 K and feed composition = 10% hydrogen, 20% isobutane, and 400 ppm of isobutylene. Helium was used as balance in all cases. Symbols: (△) propane; (□) *n*-butane; (○) isopentane.

Low fractional conversions of isobutane for the present study (below 1%) favor stable catalyst performance. For example, Corma *et al.* (41) showed that a significant deactivation did not occur for isobutane conversion over USY zeolites at 573 K when the initial conversion was kept below 5%. Similarly, Stefanadis *et al.* (38) reported good

reproducibility for isobutane conversion over HZSM-5 at 723 K if the conversion was kept below 1%.

The USY zeolite begins to deactivate with time on stream at lower temperatures (523 K) and lower concentrations of isobutane (20%). Figure 1b shows that the rates of production of alkanes decrease sharply with time on stream for isobutane conversion at 523 K, with 20% isobutane, 10% hydrogen, and 400 ppm of isobutylene in the feed. Concurrently, the apparent rates of production of olefins increase with time on stream. The initial low apparent rates of olefin production suggest that olefins are being converted into coke on the catalyst instead of desorbing into the gas phase. Coke deactivates the catalyst, as noted by the decrease in the rates of production of alkanes with time on stream. The USY catalyst does not show stable performance under low-temperature conditions (523 K), low concentrations of isobutane (20%), and high concentrations of feed isobutylene (400 ppm). Fogash *et al.* (46) have reported catalyst deactivation at higher olefin concentrations in the feed for isobutane conversion over H-mordenite at 473 K, and, similarly, Engelhardt (44) noted that the addition of olefins during isobutane conversion over H-mordenite at 573 K led to catalyst deactivation.

Figure 2 shows the rates of production of *n*-butane versus time on stream for isobutane conversion at 523 and 573 K and for isobutane inlet concentrations of 20 and 80%. The rate of production of *n*-butane remains constant with time on stream. This behavior pertains to all other products, paraffins, and olefins. In general, we achieve stable catalyst performance for isobutylene concentrations up to 400 ppm when the feed contains 80% isobutane. In addition, we maintain stable catalyst performance for isobutylene concentrations up to 400 ppm when the feed contains 20% isobutane at the higher temperature of 573 K. At the lower isobutane concentration of 20% and the lower temperature of 523 K, we obtain stable catalyst performance only for isobutylene concentrations up to 200 ppm.

Once we established the experimental conditions, we tested the reproducibility of the kinetics data. As an example, the deviations of the rates of production for propane,

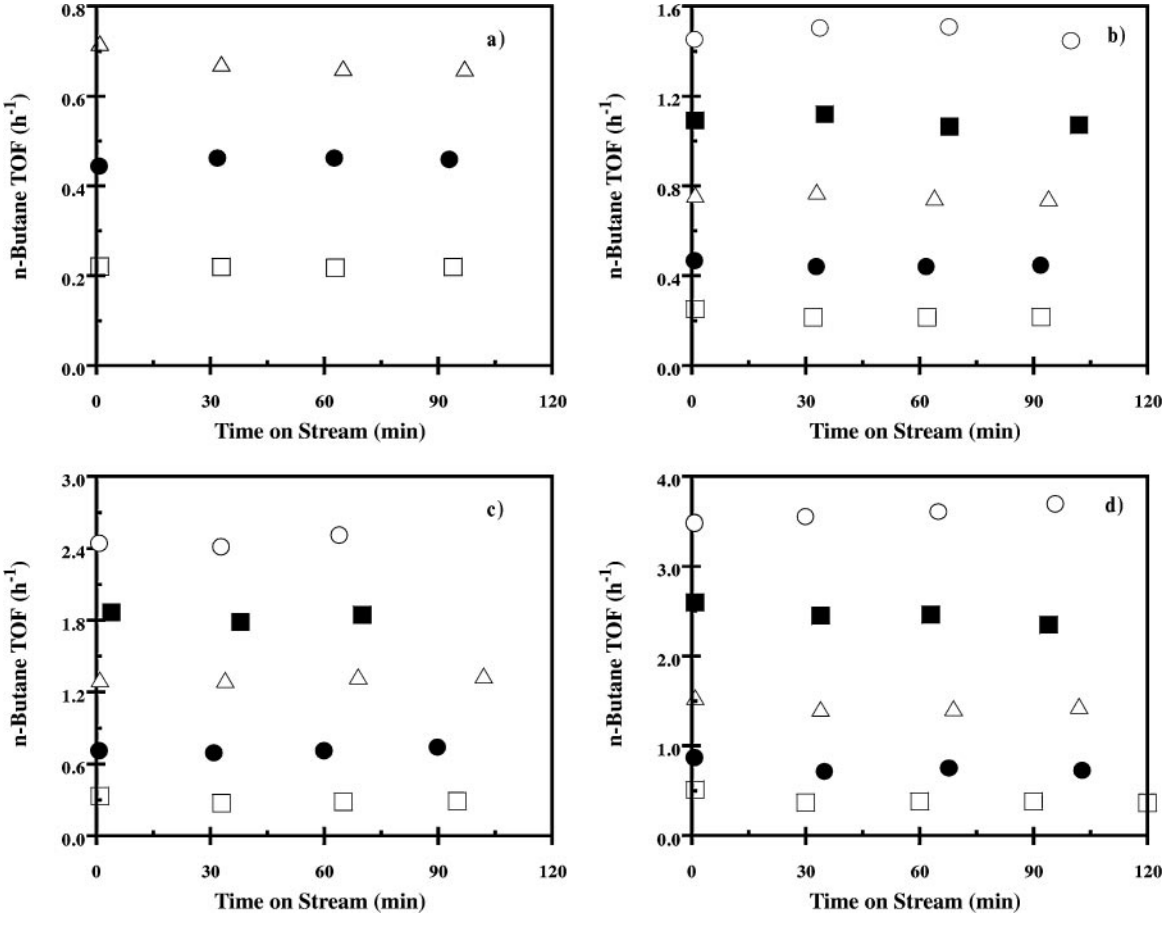

FIG. 2. *n*-Butane TOF as a function of time on stream at (a) 523 K, 10% H_2, and 20% isobutane in the feed; (b) 573 K, 10% H_2, and 20% isobutane in the feed; (c) 523 K, 10% H_2, and 80% isobutane in the feed; (d) 573 K, 10% H_2, and 80% isobutane in the feed. Helium was used as balance in all cases. The nominal isobutylene feed level, given in ppm, is (□) 50; (●) 100; (△) 200; (■) 300; (○) 400. Data collected with 300 and 400 ppm of isobutylene in the feed are not included in (a) due to catalyst deactivation.

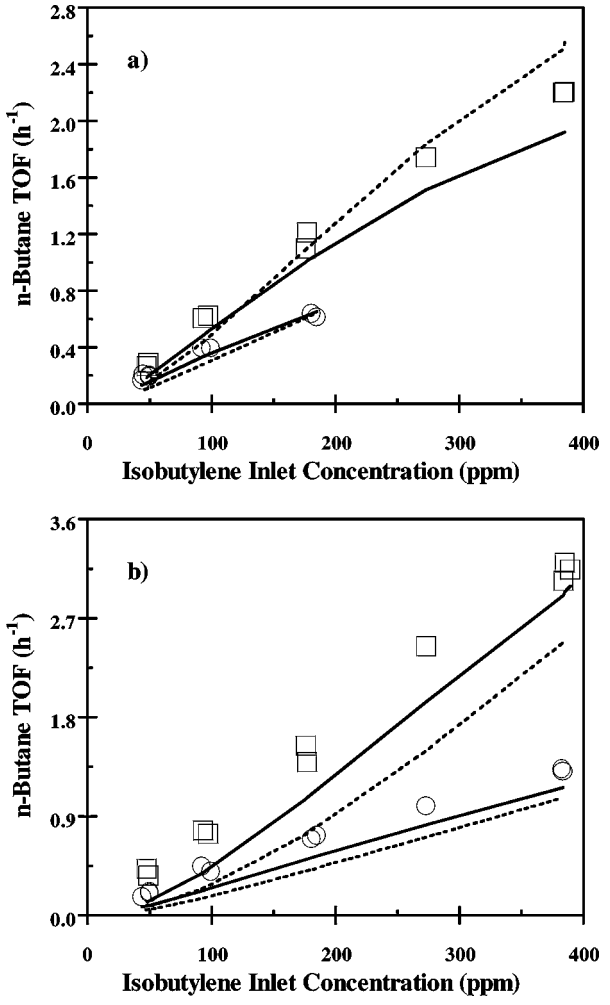

FIG. 3. *n*-Butane TOF as a function of isobutylene inlet concentration at (a) 523 K and (b) 573 K. Symbols in both figures: (○) 10% H_2 and 20% of isobutane in the feed and (□) 10% H_2 and 80% of isobutane in the feed. Helium was used as balance in both cases. The predictions of the kinetic model: solid line = full model; dotted line = simplified model.

n-butane, and isopentane were ±5.2, 5.6, and 11.3%, respectively, for five replicate experiments conducted at 523 K, with a feed composition of 20% isobutane, 10% hydrogen, and 50 ppm isobutylene.

Effect of Hydrogen

We studied the possible effect of hydrogen by comparing the rates of formation of products at 523 K, with a feed composition of 20% isobutane, 50 ppm of isobutylene, and concentrations of hydrogen equal to 10 and 80%. These experiments showed that an eightfold increase in hydrogen concentration had a minor effect on catalyst performance, indicating that our USY catalyst does not show hydrogenation–dehydrogenation activity under the present reaction conditions. Fogash *et al.* (46) also reported a negligible effect of hydrogen concentration (10 and 50%) on isobutane conversion over H-mordenite at 473 K. Bearez *et al.* (51) indicated that hydrogen had no effect on *n*-butane conversion over H-mordenite at 623 K. However, Asuquo *et al.* (24) observed a slight inhibiting effect of hydrogen on the rate of *n*-butane conversion over H-mordenite at 523 K.

Rates of Production of Paraffins and Olefins

Figures 3–5 show the effects of temperature, isobutane inlet concentration, and isobutylene feed concentration on the rates of production of *n*-butane, propane, and isopentane. An increase of isobutylene feed concentration increases the TOFs of *n*-butane, propane, and isopentane production at temperatures of 523 and 573 K for isobutane concentrations of 20 and 80% (Fig. 3). The rates

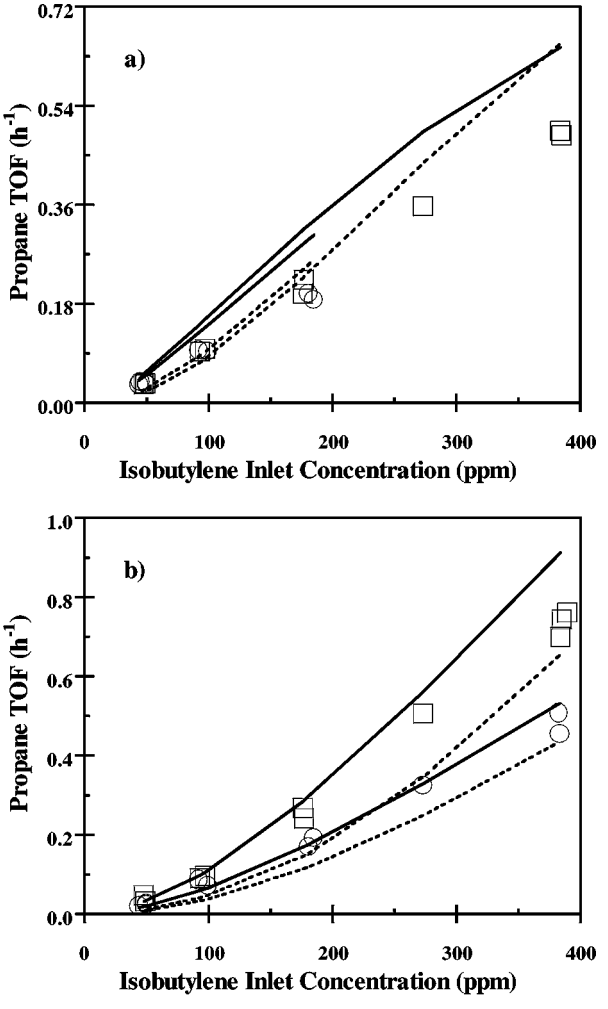

FIG. 4. Propane TOF as a function of isobutylene inlet concentration at (a) 523 K and (b) 573 K. Symbols in both figures: (○) 10% H_2 and 20% of isobutane in the feed and (□) 10% H_2 and 80% of isobutane in the feed. Helium was used as balance in both cases. The predictions of the kinetic model: solid line = full model; dotted line = simplified model.

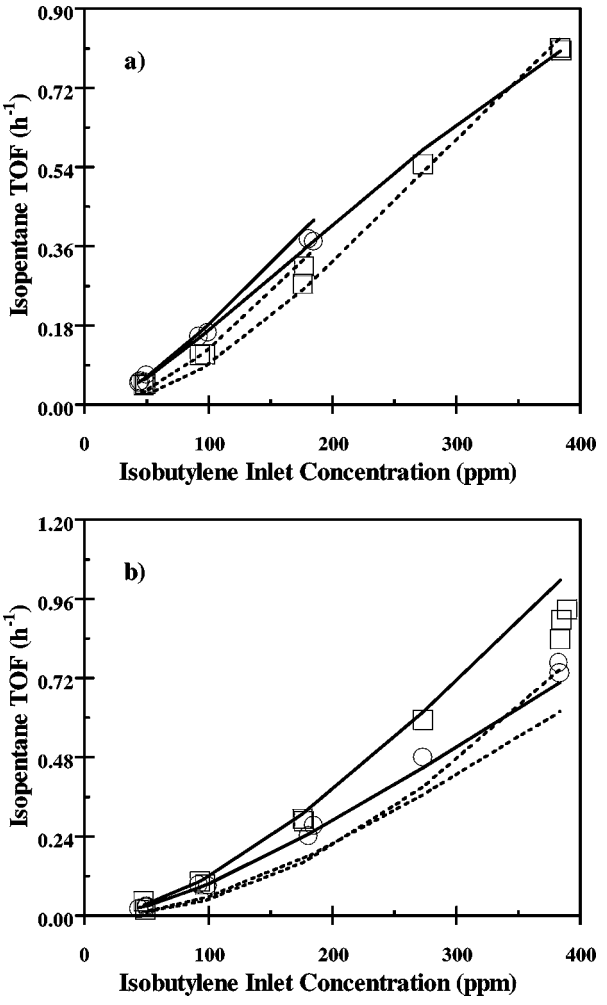

FIG. 5. Isopentane TOF as a function of isobutylene inlet concentration at (a) 523 K and (b) 573 K. Symbols in both figures: (○) 10% H_2 and 20% of isobutane in the feed and (□) 10% H_2 and 80% of isobutane in the feed. Helium was used as balance in both cases. The predictions of the kinetic model: solid line = full model; dotted line = simplified model.

of *n*-butane and propane formation are higher with 80% isobutane, especially at a temperature of 573 K, with the effect of the isobutane concentration being more important for *n*-butane formation. This effect is smallest for isopentane formation (Fig. 5).

Figures 6 and 7 show the effects of temperature, isobutane inlet concentration, and isobutylene feed concentration on the rates of olefin production. Increasing the isobutylene feed concentration increases the rates of production of propylene and *n*-butylene (i.e., sum of 1-butylene, *trans*-2-butylene, and *cis*-2-butylene) in all cases. However, unlike alkane formation, increasing the concentration of isobutane in the feed decreases the TOF of propylene and *n*-butylene formation. This behavior is due to higher rates of hydride transfer reactions at higher isobutane inlet concentrations.

DEVELOPMENT OF THE KINETIC MODEL

Background

Various approaches have been used to develop kinetic models of hydrocarbon conversion processes over solid acid catalysts. For example, the components of the reaction may be lumped as a function of their physical or chemical properties, and the reaction network is then defined in terms of chemical interactions between lumps. Essential aspects of the chemistry have been included into a lumped model by Liguras and Allen (52, 53) and Quann and Jaffe (54, 55). Other studies (56–58) have generated the elementary steps of a complex reaction network by using computer algorithms based on chemical rules. In this respect, Froment *et al.* (59–62) have described the generation of reaction networks using a computer algorithm in which each species is

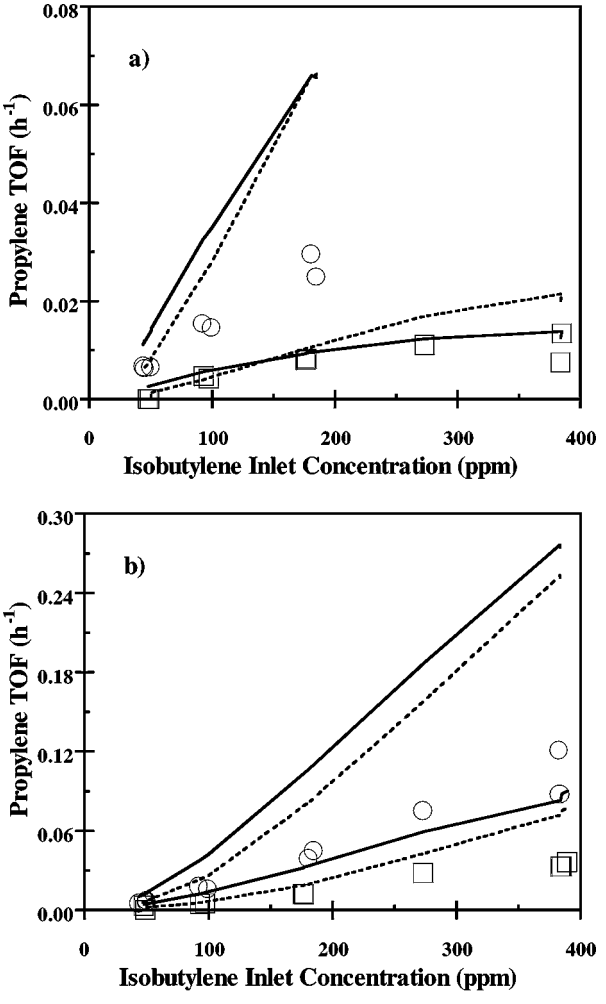

FIG. 6. Propylene TOF as a function of isobutylene inlet concentration at (a) 523 K and (b) 573 K. Symbols in both figures: (○) 10% H_2 and 20% of isobutane in the feed and (□) 10% H_2 and 80% of isobutane in the feed. Helium was used as balance in both cases. The predictions of the kinetic model: solid line = full model; dotted line = simplified model.

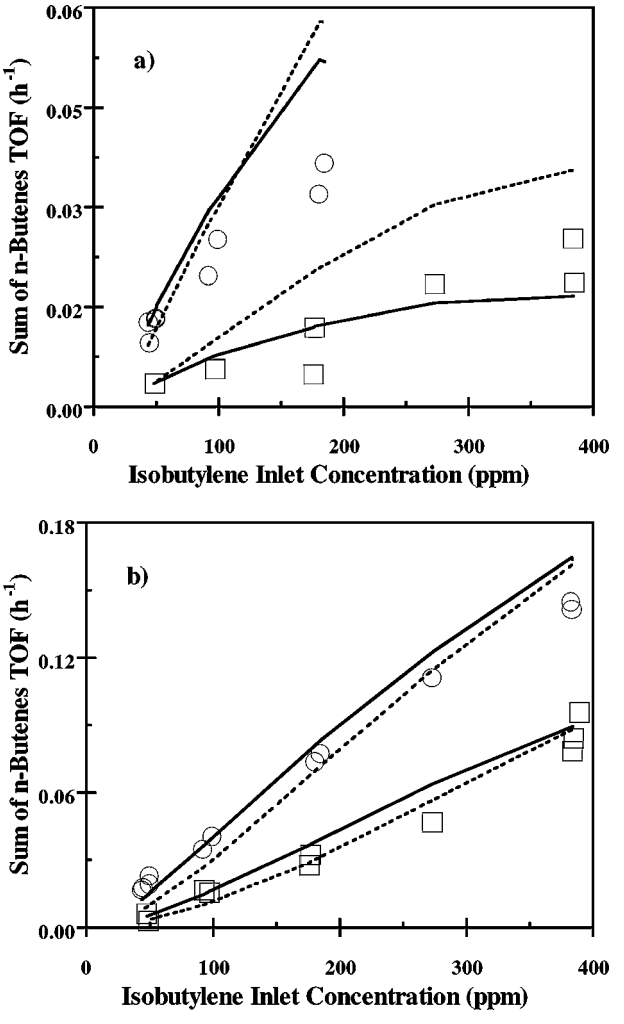

FIG. 7. Sum of *n*-butenes TOF as a function of isobutylene inlet concentration at (a) 523K and (b) 573 K. Symbols in both figures: (○) 10% H_2 and 20% of isobutane in the feed and (□) 10% H_2 and 80% of isobutane in the feed. Helium was used as balance in both cases. The predictions of the kinetic model: solid line = full model; dotted line = simplified model.

represented by a Boolean relationship matrix. The rate constant of each elementary step is calculated as the product of the number of single events and the so-called single-event rate coefficient. This approach has the advantage that the single-event rate coefficient is independent of the feedstock and may be determined for each catalyst by experiments with selected probe molecules.

Yaluris *et al.* (42, 43) developed a model based on initiation steps, β-scission, oligomerization, isomerization, olefin desorption, and hydride transfer reactions for isobutane conversion over a series of calcined and steamed USY-based fluid catalytic cracking (FCC) catalysts, at temperatures between 733 and 773 K. Yaluris *et al.* later extended this model (26) to describe the cracking of 2-methylhexane on USY catalysts with different Brønsted acid strengths. The chemistry for the cracking of 2-methylhexane is essentially the same as that for isobutane cracking, with the primary difference being that the larger 2-methylhexane reactant has more reaction pathways available to it than isobutane. Fogash *et al.* (46), by feeding ppm levels of isobutylene at 473 K on H-mordenite to form isobutyl-reactive intermediates, formulated a model for isobutane conversion without the need for initiation reactions, and included only adsorption, oligomerization, β-scission, isomerization, and hydride transfer reactions.

The model we develop here is based on the kinetic models of Yaluris *et al.* (42, 43) for hydrocarbon conversion reactions on solid acid catalysts. This model, based on a surface chain reaction scheme, involves initiation, propagation, and termination steps. However, there are distinct and important differences between the current model and the earlier work described by Yaluris *et al.* (42, 43). The latter model assumed that reactive intermediates on the acid sites were carbenium ions, whereas the present model assumes that these species are neutral alkoxy species. We have shown elsewhere that the two approaches are kinetically equivalent, and the model results are the same with either set of assumptions (63). If the reactive intermediates are assumed to be carbenium ions, then the heats of reactions for the various elementary steps change with the acid strength of the catalyst; and, since the transition states would also be carbenium ions, the activation energies should remain constant. In contrast, if the reactive intermediates are assumed to be neutral alkoxy species, then the heats of reactions for the various elementary steps remain constant; however, since the transition states are assumed to be carbenium ions in this case, the activation energies change with the acid strength of the catalyst. Since it is now established that adsorbed species formed in initiation processes are surface alkoxy species instead of surface carbenium ions (64–67), we base our current kinetic model on this assumption. The reactions of these neutral surface alkoxy species take place through carbenium ion transition states (65–67), thereby explaining why selectivity patterns displayed in the reactions of hydrocarbons over solid acid catalysts are controlled by the relative stabilities of tertiary, secondary, and primary carbenium ions.

The earlier treatment of Yaluris *et al.* (42) used the enthalpy of stabilization of a carbenium ion relative to a surface proton as a key representation of the catalytic site; a single value was used for all carbenium ions. Here we utilize the results from recent experimental studies, which indicate that the heats of adsorption for various alkanes in zeolites vary linearly with carbon number (5, 68–71). Accordingly, the heats of adsorption for various olefins to form alkoxy species in zeolites should also vary linearly with carbon number. Specifically, the formation of a surface alkoxy species from a gaseous olefin can be written as the formation of an adsorbed precursor olefin, followed by the formation of the alkoxy species upon the transfer of a

hydrogen atom from the zeolite to the adsorbed precursor olefin. The stabilization of the adsorbed precursor olefin in the zeolite should correlate with the stabilization of the corresponding alkane, and the heat of hydrogen transfer from the zeolite to the adsorbed precursor olefin should be rather insensitive to the hydrocarbon chain length. This dependence on chain length for the stabilization of hydrocarbon species within zeolites was recently included in various analyses of hydrocarbon cracking reactions (72, 73).

Formulation of the Kinetic Model

First, we define the set of adsorbed species in the model. Under low-temperature reaction conditions, the primary olefins observed in the reactor effluent are isobutylene, 1-butylene, *cis*- and *trans*-2-butylene, propylene, and smaller amounts of 2-methyl-butylenes. Accordingly, these olefins adsorb to form the following species:

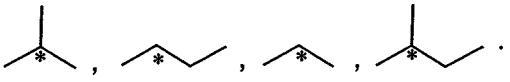

Next, we allow these adsorbed species to oligomerize with the primary olefins observed in the reactor effluent:

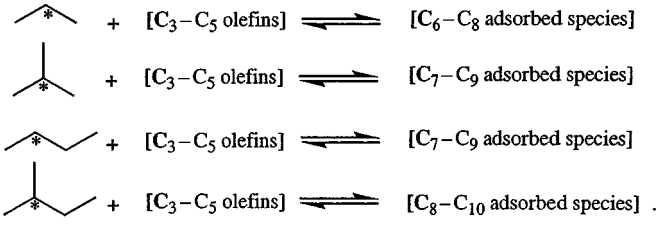

We write these oligomerization steps in accord with Markovnikov's rule as

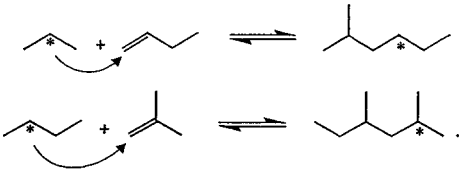

This makes C_{10} species the heaviest hydrocarbon species on the catalyst. However, since C_4 olefins are the most abundant in the reactor, we expect surface species as heavy as C_{12} to form from the oligomerization of three C_4 species. Therefore, we add the following oligomerization steps, truncating all possible adsorbed species at 12 carbon atoms:

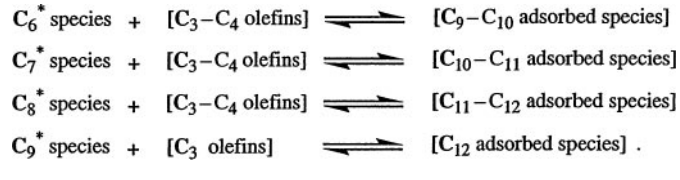

This approach leads to 106 steps for oligomerization and β-scission processes, involving 90 adsorbed hydrocarbon species. While the choice of these steps is somewhat arbitrary, we show later that relatively few of these steps are kinetically significant.

The reaction scheme is next expanded by allowing adsorbed alkoxy species to be formed via adsorption of the corresponding olefin on a Brønsted acid site, as illustrated in the following for isobutyl and *n*-butyl species:

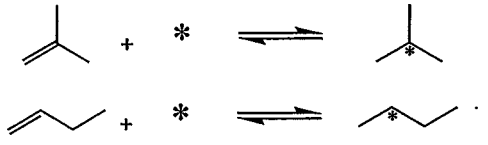

The 90 adsorbed species lead to the addition of 94 adsorption–desorption steps. Three C_4 olefins are generated from adsorbed *n*-butyl species. We have allowed two C_5 olefins to be formed from adsorbed isopentyl species and two C_6 olefins to be formed from adsorbed isohexyl species. We note that the formation of surface isobutyl species from the adsorption of isobutylene represents the primary initiation route for isobutane conversion at temperatures below 573 K.

The 90 adsorbed hydrocarbon species may be interconverted through isomerization steps. As outlined in the following section, the results from our model suggest that isomerization steps are quasi-equilibrated, i.e., the forward and reverse rates of each step are significantly faster than the net rate. Therefore, it is not necessary to write all possible isomerization steps. Instead, it is sufficient to include steps whereby each adsorbed hydrocarbon species with a given number of carbon atoms can be converted to each isomer of this species, either directly or via a sequence of isomerization steps. We have included 79 representative isomerization steps, involving branching and nonbranching rearrangements, to allow interconversion between the various C_n^* isomers.

The reaction scheme also contains 89 steps representing hydride transfer for each surface species (with the exception of isobutyl species) with isobutane, for example,

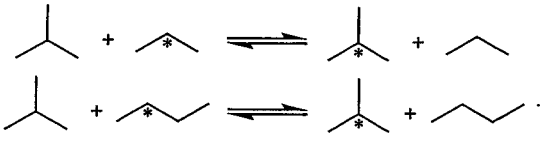

Finally, we include two initiation steps for the activation of isobutane at higher temperatures to form surface isobutyl species or surface propyl species (i.e., initiation processes at high temperatures),

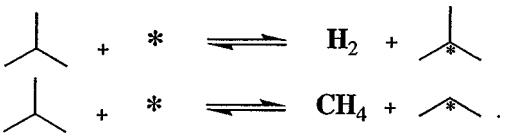

In summary, our kinetic model for isobutane conversion over a solid acid catalyst, under the conditions of our study, contains 370 steps, which combine to form surface chain reaction cycles. This reaction scheme involves 2 initiation steps for isobutane activation, 94 steps for olefin adsorption/desorption processes, 106 steps for oligomerization/β-scission steps involving olefins and adsorbed species, 79 isomerization steps for interconversion of adsorbed C_n^* isomers, and 89 hydride transfer reactions of adsorbed species with isobutane (leading to propagation as well as termination of surface chain reactions). We again note that one of the adsorption steps, adsorption of isobutylene from the reactor feed, initiates isobutane conversion at low temperatures. The Appendix outlines the algorithm used to generate the elementary steps included in our model.

Parameterization of the Kinetic Model

Thermodynamic properties. For each family of reactions described in the previous section, we parameterize the model in terms of either the forward or the reverse rate constant ($k_{i,\text{for}}$ or $k_{i,\text{rev}}$), which are related to the thermodynamic equilibrium constant ($K_{i,\text{eq}}$),

$$\frac{k_{i,\text{for}}}{k_{i,\text{rev}}} = K_{i,\text{eq}}. \qquad [1]$$

We therefore need to calculate $K_{i,\text{eq}}$ for each of the 370 steps of the reaction sequence. And since

$$K_{i,\text{eq}} = \exp\left(\frac{\Delta S_i^\circ}{R} - \frac{\Delta H_i^\circ}{RT}\right), \qquad [2]$$

we need to estimate standard entropy and enthalpy changes (ΔS_i° and ΔH_i°) from the thermodynamic properties of the gaseous and surface species. R and T are the gas constant and temperature, respectively.

As a first step we need to consider the reaction thermodynamics of the system and estimate the absolute entropies and enthalpies of formation for all gaseous olefins and paraffins in their standard states (i.e., at 1 atm and at the reactor temperature). These values may be found in standard references for the lighter hydrocarbons (C_n species with $n < 7$). For heavier hydrocarbons, we use Benson's group contribution methods (74–77). Importantly, by basing the kinetic model on thermodynamic values for gaseous species (including the reactants and the observed products), we ensure that all kinetic parameters of the model will be thermodynamically consistent.

Next, we estimate the thermodynamic properties of all surface species in terms of standard entropy changes and enthalpy changes of adsorption for all gaseous olefins. The model contains 94 steps for olefin adsorption/desorption; and, we use these steps to relate the thermodynamic properties of all adsorbed species to the known thermodynamic properties of gaseous olefins. As noted earlier, the heats of adsorption for various alkanes in zeolites vary linearly with carbon number (5, 68–71). Accordingly, we define the enthalpy of formation for a surface species as

$$H^\circ_{\text{surface}} = H^\circ_{\text{olefin}} + \Delta H_3^\circ + \alpha_H(N_c - 3), \qquad [3]$$

where H°_{surface} and H°_{olefin} are the enthalpies of formation of the surface species and the corresponding gaseous olefin; ΔH_3° is the enthalpy change of adsorption for propylene; N_c is the number of carbon atoms in the surface species; and α_H is the slope of the linear variation of the adsorption heat with carbon number. The value of ΔH_3° can be estimated based on the results of theoretical calculations. For example, a value of -87.1 kJ mol^{-1} has been calculated by Kazansky *et al.* (78) for the heat of adsorption of isobutylene on a cluster emulating the properties of an acid site on an aluminosilicate compound. Also, Natal-Santiago *et al.* (67) reported a value of about -80 kJ mol^{-1} for the adsorption of C_6-olefins to form hexyl species on an aluminosilicate site. We thus selected a value of -90 kJ mol^{-1} for ΔH_3°. Importantly, the parameter ΔH_3° is not kinetically significant at a value of -90 kJ mol^{-1}, since the surface coverages by adsorbed species remain low for this value under the reaction conditions of the present study. Accordingly, the value of ΔH_3° was fixed in all kinetic analyses. Hence, the enthalpies of all surface species are defined in terms of one parameter: α_H.

The estimation of standard entropies for all surface species is based on the local entropies of gaseous olefins and the changes in symmetry that occur upon adsorption. The local entropy, S_{loc}, of a gaseous species is calculated by subtracting the gaseous translational entropy, $S^\circ_{trans3D}$, from the total entropy (leaving the entropy contributions from vibrational and rotational degrees of freedom). To account for the changes in symmetry upon adsorption, we again use Benson's method to estimate standard entropies for unknown species in terms of known species. This method has been used extensively by Froment and co-workers in their detailed analyses of hydrocarbon reactions over various catalysts (59). The basis for the effects of symmetry is outlined in the following.

The absolute entropy, S, of a molecule is given by

$$S = R\ \ln\Omega, \qquad [4]$$

where Ω is the number of distinguishable configurations of the compound. In this expression, the rotational entropy contributions must be corrected to account for the indistinguishable configurations of the molecule due to symmetry. Thus a term ($R\ \ln\sigma_s$) must be subtracted from the entropy

expression above, where σ_s is the symmetry number of the molecule. In addition, if the molecule has optical isomers (i.e., it contains one or more asymmetric carbon atoms), then the number of spatial orientations is increased, and the entropy is increased by a term ($R\ \ln 2^n$), where n is the number of chiral carbon atoms. Therefore, the absolute entropy for the species is given by

$$S = R\ \ln\Omega' + R\ \ln(2^n/\sigma_s), \qquad [5]$$

where Ω' is the number of configurations of the compound without regard to symmetry.

We now use the previous expression to relate the entropy of an adsorbed species, S_{surface}, to the standard entropy of a corresponding gaseous species, S°_{gas},

$$S_{\text{surface}} = F_{\text{loc}}\left\{(S^{\circ}_{\text{gas}} - S^{\circ}_{trans,3D}) + R\ \ln\left(\frac{2^{n_{\text{surface}}}}{\sigma_{\text{surface}}}\right) - R\ \ln\left(\frac{2^{n_{\text{gas}}}}{\sigma_{\text{gas}}}\right)\right\}, \qquad [6]$$

where the subscripts "surface" and "gas" refer to the symmetry numbers and the numbers of chiral centers in the surface species and the gaseous olefin, respectively. The term F_{loc} corresponds to the fraction of the local entropy in the gaseous molecule that is retained by the surface species. We have now defined the entropies of all surface species in terms of one parameter: F_{loc}.

Adsorption–desorption. For the adsorption/desorption family of steps, we choose to define the rate constants in terms of the adsorption direction. Accordingly, we define the adsorption rate constant from collision theory as

$$k_{\text{ads}} = \frac{\exp\left(-\frac{E_{\text{ads}}}{RT}\right)}{\sqrt{2\pi m_{\text{A}} k_{\text{B}} T}} A_{\text{site}}, \qquad [7]$$

where E_{ads} is the activation energy for adsorption and A_{site} is the area occupied per site. In these analyses, we have used a value for A_{site} of 10^{-15} cm^2/site, corresponding to a typical molecular cross-sectional area. We then use the equilibrium constant for the step to calculate the desorption rate constant. Typical values for E_{ads} estimated from DFT calculations range from 10 to 50 kJ mol^{-1} (78–80). Since the adsorption–desorption steps become quasi-equilibrated for a value of E_{ads} equal to 50 kJ mol^{-1}, this value is not kinetically significant. (Specifically, the value of E_{ads} can be lower than 50 kJ mol^{-1} without having any effect on the predictions of the kinetic model.) Therefore, we have fixed E_{ads} to be equal to the value of 50 kJ mol^{-1} taken from DFT calculations.

Initiation. We calculate two rate constants, k_{init}, for initiation of the reaction by activation of isobutane (to produce adsorbed isobutyl and adsorbed propyl species) in the same manner as the adsorption steps, i.e., using a collision theory for the forward direction,

$$k_{\text{init}} = \frac{\exp\left(-\frac{E_{\text{init}}}{RT}\right)}{\sqrt{2\pi m_{\text{A}} k_{\text{B}} T}} A_{\text{site}}, \qquad [8]$$

where E_{init} is the activation energy for the initiation reaction. We use a slightly different value of E_{init} for the initiation reaction to form adsorbed isobutyl species and hydrogen ($E_{\text{init, H}_2}$) than for the reaction to form adsorbed propyl species and CH_4 ($E_{\text{init, CH}_4}$).

Oligomerization/β-scission. For the oligomerization/β-scission family of steps, we choose to define the rate constants in terms of the β-scission direction. Since this direction for the reactions does not involve gaseous species, we write the rate constant for β-scission, k_β, as

$$k_\beta = 10^{13} \exp\left(-\frac{E_\beta}{RT}\right), \qquad [9]$$

where E_β is the activation energy for β-scission. The value of E_β depends on the nature of the β-scission process. Specifically, we expect the order for values of E_β to be

$$E_{\beta,\text{ss}} > E_{\beta,\text{st}} > E_{\beta,\text{tt}},$$

where $E_{\beta,\text{ss}}$ corresponds to the activation energy for β-scission of a secondary species to form another secondary species; $E_{\beta,\text{st}}$ corresponds to β-scission of a secondary species to form a tertiary species or β-scission of a tertiary species to form a secondary species; and $E_{\beta,\text{tt}}$ corresponds to β-scission of a tertiary species to form another tertiary species. We fix the value of the pre-exponential factor to a typical value of 10^{13} s^{-1}, which corresponds to the situation where the entropy of the activated complex is equal to that of the adsorbed reactant species. Accordingly, we initially parameterize the rate constants for the 106 β-scission steps in terms of three kinetic parameters: $E_{\beta,\text{ss}}$, $E_{\beta,\text{st}}$, and $E_{\beta,\text{tt}}$.

Isomerization. The rate constants for the isomerization families of steps are similar in both the forward and the reverse directions. For convenience, we choose to parameterize the kinetic model in terms of the forward rate constants. The rate constants for isomerization steps are written as

$$k_{\text{iso}} = 10^{13} \exp\left(-\frac{E_{\text{iso}}}{RT}\right), \qquad [10]$$

where E_{iso} is the activation energy for the isomerization step. Kramer *et al.* (13) have measured a value of about 60 kJ mol^{-1} for the activation energy of the nonbranching isomerization of 2-methyl-2-pentene over a USY zeolite catalyst. Natal-Santiago *et al.* (67) have estimated that the activation energy for the branching rearrangement of 2-methyl-2-pentene is about 50 kJ mol^{-1} higher than that for the nonbranching rearrangement. In addition, DFT

studies of branching rearrangements indicate that the activation energy for isomerization of an *n*-alkoxy to an iso-alkoxy species is near 126 kJ mol^{-1} (81). Furthermore, the activation energy for branching isomerization of hexyl species on ZSM-5 has been estimated to vary between 130 and 140 kJ mol^{-1} (80). Therefore, we have used values of E_{iso} equal to 80 and 110 kJ mol^{-1} for nonbranching and branching isomerization reactions, respectively. We note, however, that the values of E_{iso} for the isomerization steps are not kinetically significant, because these steps are predicted to be quasi-equilibrated under the reaction conditions of this study.

Hydride transfer. We parameterize the hydride transfer family of steps in the direction of the reaction with isobutane. Accordingly, we define the hydride transfer rate constant, k_H, from collision theory as

$$k_H = \frac{\exp\left(-\frac{E_H}{RT}\right)}{\sqrt{2\pi m_A k_B T}} A_{site} \exp\left(\frac{\Delta S^{\ddagger}}{R}\right), \qquad [11]$$

where E_H is the activation energy for hydride transfer and $\Delta S^{\ddagger}$ is an entropy change related to the formation of the activated complex. We note that if $\Delta S^{\ddagger}$ is equal to zero, then the expression for the rate constant is given by the collision rate of isobutane molecules on the acid sites times the probability that these collisions surmount the activation energy barrier. It can be shown (e.g., 82) that the formation of the transition state from the gas phase for this case corresponds to the loss of one degree of translation (perpendicular to the surface). Since this situation corresponds to the maximum rate of adsorption, it follows that the maximum value of $\Delta S^{\ddagger}$ is equal to zero, and negative values of $\Delta S^{\ddagger}$ correspond to the loss of entropy from the maximum possible value. We have included $\Delta S^{\ddagger}$ as a kinetic parameter, since the values of k_H have high sensitivity in the kinetic analysis. We are neither able to achieve a proper value of k_H nor describe correctly the temperature dependence of k_H with a single kinetic parameter, E_H. In our kinetic analysis, we allow different values of E_H for hydride transfer of isobutane with propyl species, *n*-butyl species, isopentyl species, and all heavier species, and we use the same $\Delta S^{\ddagger}$ value for all hydride transfer steps. Therefore, we parameterize the rate constants for the 89 hydride transfer steps in terms of five kinetic parameters: E_{C_3}, E_{C_4}, E_{C_5}, $E_{C>5}$, and $\Delta S^{\ddagger}_{Hydride}$.

Summary of Model Development

The reaction scheme outlined previously leads to a kinetic model containing 277 unknowns (i.e., 186 gaseous molecular flow rates, 90 surface species, and the fraction of free sites). We have assumed that the reactor operates as a plug-flow reactor. Therefore, we solve 186 differential equations for the gaseous molecular flow rates versus reactor length, combined with 90 steady-state equations for the fractional surface coverages by adsorbed species and 1 site-balance equation. The number of unknowns may be decreased to 192 by lumping the $C_{>5}$ paraffins as a single species, and the number of differential equations to be solved for gaseous molecular flow rates decreases from 186 to 101. We initially use 12 kinetic parameters that are kinetically significant to describe the model: α_H, F_{loc}, E_{init,H_2}, E_{init,CH_4}, $E_{\beta,tt}$, $E_{\beta,st}$, $E_{\beta,ss}$, E_{C_3}, E_{C_4}, E_{C_5}, $E_{C>5}$, and $\Delta S^{\ddagger}_{Hydride}$.

RESULTS OF THE KINETIC MODEL

We used the kinetic model to reconcile reaction kinetics data collected in the present study at low temperatures with reaction kinetics data collected previously at higher temperatures (42). The values of the kinetic parameters used to describe the reaction kinetics data under both sets of reaction conditions are summarized in Table 2. It was found that the values for $E_{\beta st}$ and $E_{\beta ss}$ were very similar, and hence we used the same value for both parameters. This constraint reduces the number of kinetic parameters to 11. Values for the fitted parameters were determined using Athena Visual Workbench engineering software (83). Importantly, Table 2 also gives the 95% confidence limits for the kinetic parameters. In addition to adjusting these parameters, it was necessary to adjust the rate constants for two of the oligomerization steps (steps 8 and 9 in Table 3) by a factor of 0.45. This correction was done based on a sensitivity analysis (to be discussed later). Considering the size and complexity of the model, we rationalize this small adjustment as a correction for errors in evaluation of the rate constants.

The results from our kinetic model give similar activation energies for the two initiation steps representing the activation of isobutane to form surface isobutyl species and surface propyl species, i.e., values of 156.5 and 154.3 kJ mol^{-1},

TABLE 2

Values and Confidence Limits for Kinetic Parameters[a]

Parameter	Value	95% Confidence interval
α_H	−0.54	−1.66–0
F_{loc}	1.17	±0.01
E_{init,H_2}	156.5	±0.5
E_{init,CH_4}	154.3	±0.5
$E_{\beta,tt}$	102.2	±5.8
$E_{\beta,st} = E_{\beta,ss}$	115.1	±5.7
E_{C_3}	64.3	±1.4
E_{C_4}	76.5	±1.4
E_{C_5}	62.2	±1.7
$E_{C>5}$	62.2	±1.4
$\Delta S^{\ddagger}_{Hydride}$	−24.3	±2.2

[a] α_H, enthalpy changes, and activation energies are given in kJ mol^{-1}, and entropy changes in J mol^{-1} K^{-1}. The other parameters are dimensionless.

respectively. These values are in close agreement with the activation energies reported in the previous kinetic model by Yaluris *et al.* (42, 43) (i.e., 162.6 and 159.2 kJ mol^{-1}, respectively); however, they are lower than the activation energies estimated from DFT calculations (78) (i.e., 279.6 and 240.6 kJ mol^{-1}).

The value of $E_{\beta,tt}$ (102.2 kJ mol^{-1}) (Table 2) is lower than the value of $E_{\beta,st}$ and $E_{\beta,ss}$ (115.1 kJ mol^{-1}). These activation barriers for β-scission are higher than previous estimates from Yaluris *et al.* (42). Martens *et al.* (73) reported higher activation barriers for the β-scission of C_8^* species, i.e., values of 180, 188.5, and 184 kJ mol^{-1} for $E_{\beta,ss}$, $E_{\beta,st}$, and $E_{\beta,tt}$, respectively. However, these authors used higher values for the heats of adsorption of olefins (from −110 to −150 kJ mol^{-1}) than those used in the present study. Accordingly, the higher activation energy barriers for β-scission used by Martens *et al.* compared to the present model are compensated by more exothermic heats of adsorption to form the surface alkoxy species from gaseous olefins.

According to the kinetic model, the surface of the USY zeolite catalyst is mostly composed of vacant acid sites under reaction conditions for isobutane conversion, i.e., approximately 99% or greater of the acid sites are free under all reaction conditions. For both sets of reaction conditions, the most abundant surface species are predicted to be *n*-butyl species and isobutyl species. Other species with significant surface concentrations are the isopentyl and propyl species. The most abundant heavy species are predicted to be C_6^*, C_7^*, and C_8^* species. The fractional surface coverage by adsorbed C_9^*–C_{12}^* species is very low (e.g., 10^{-8}), which is consistent with our assumption to neglect surface species heavier than C_{12}^* species.

Figures 3–7 show the trends for the rates of production of *n*-butane, propane, isopentane, propylene, and *n*-butylenes (sum of 1-butylene, *cis*- and *trans*-2-butylene) versus isobutylene feed concentration at the low temperatures of the present study. In addition, Figs. 8–10 show the rates of production of hydrogen, methane, *n*-butane, propane, isopentane, propylene, butylenes (sum of isobutylene, 1-butylene, *cis*- and *trans*-2-butylene), and 2-methyl-2-butylene versus temperature using data obtained at higher temperatures from a previous study reported by Yaluris *et al.* (42). Importantly, H_2, CH_4, and 2-methyl-2-butylene were not observed in significant amounts at lower temperatures in the present study. The solid lines in Figs. 3–10 represent predictions from the kinetic model. The kinetic model describes the trends correctly for all products at both sets of reaction conditions. For the lower temperature case, the model tends to over-predict the olefin concentrations (especially propylene) at high isobutylene concentrations in the feed. Since we have observed catalyst deactivation under these conditions, we suggest that some of the olefins, particularly propylene, are consumed in processes leading to coke, thereby causing the model to over-predict these concentrations. Lower reaction temperatures, lower concentrations of isobutane, and larger amounts of isobutylene in the feed enhance coke formation. These are the conditions under which the model predictions for the rate of propylene formation deviate most from the experimental data.

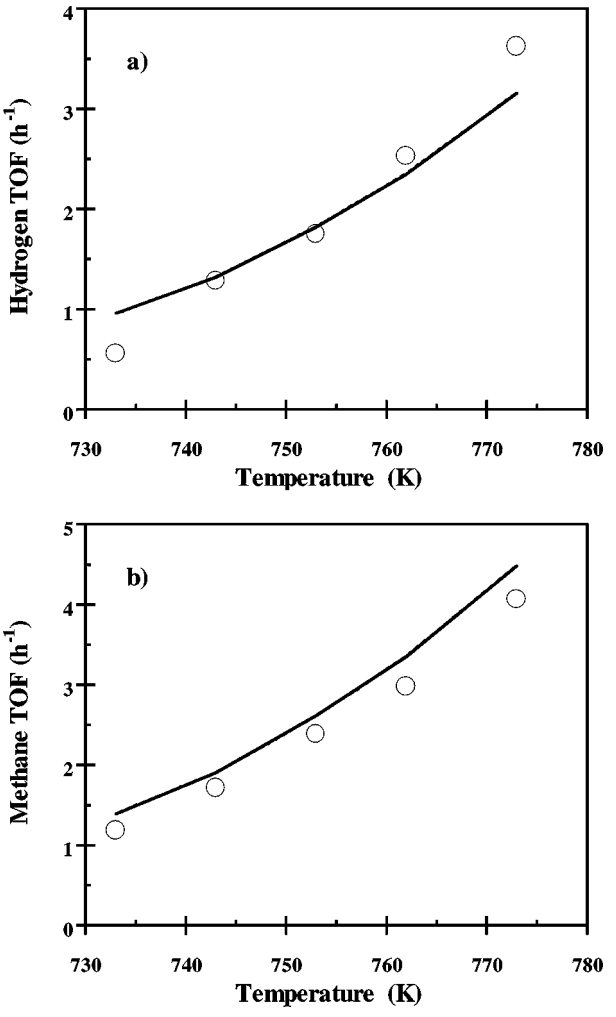

FIG. 8. (a) Hydrogen TOF and (b) methane TOF, as a function of temperature for the data set at high temperature (42). The predictions of the full kinetic model are given by solid lines. The predictions of the full and simplified models superimpose.

The good agreement between experimental results and model predictions, over the wide range of reaction conditions considered in this study, suggests that the kinetic model is able to bridge the gap between the kinetics of isobutane conversion at low and high temperatures by changing the nature of the initiation steps while maintaining the same propagation and termination steps. Results over such a large temperature range gives us confidence in the kinetic parameters of Table 2 derived by the model. These parameters will be essential for comparing and differentiating the performance of different solid acids.

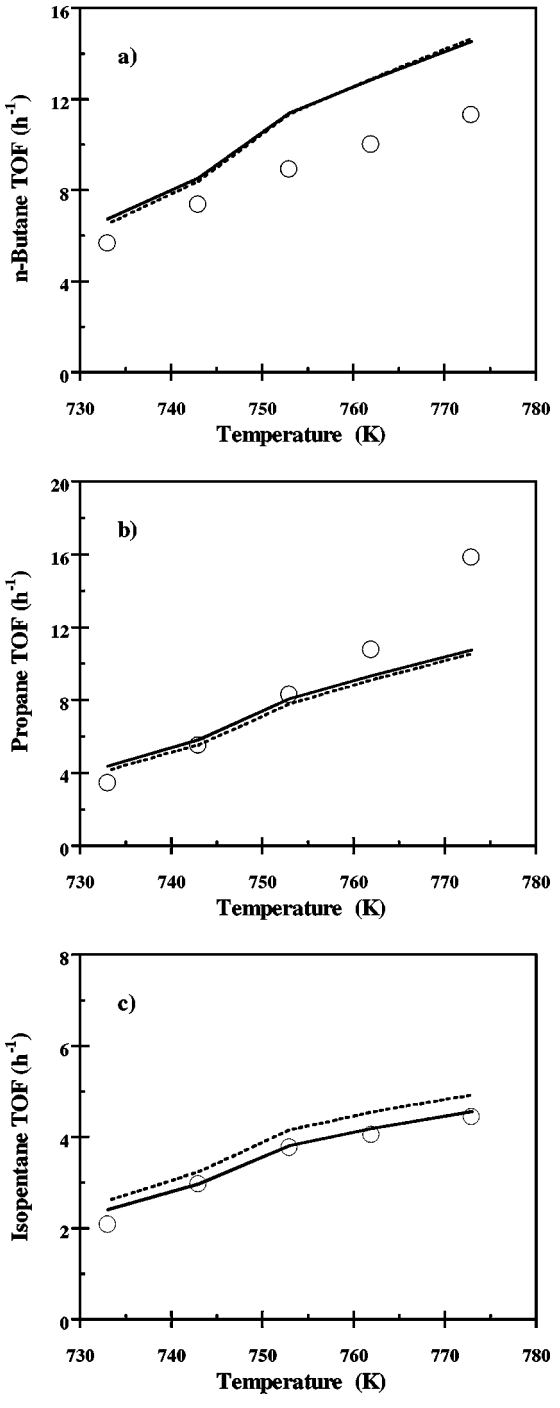

FIG. 9. (a) *n*-Butane TOF, (b) propane TOF, and (c) isopentane TOF, as a function of temperature for the data set at high temperature (42). The predictions of the kinetic model are given by: solid line = full model; dotted line = simplified model.

Sensitivity Analysis

We next consider the sensitivity of the kinetic model to various steps in the reaction scheme. Campbell's degree of rate control based on a single species, $X_{\mathrm{RC},i}$, is given by (84)

$$X_{\mathrm{RC},i} = \left(\frac{\partial r}{\partial k_{i,\mathrm{for}}}\right)_{K_{\mathrm{eq},i,k_j}} \frac{k_{i,\mathrm{for}}}{r} = \left(\frac{\partial r}{\partial k_{i,\mathrm{rev}}}\right)_{K_{\mathrm{eq},i,k_j}} \frac{k_{i,\mathrm{rev}}}{r}. \quad [12]$$

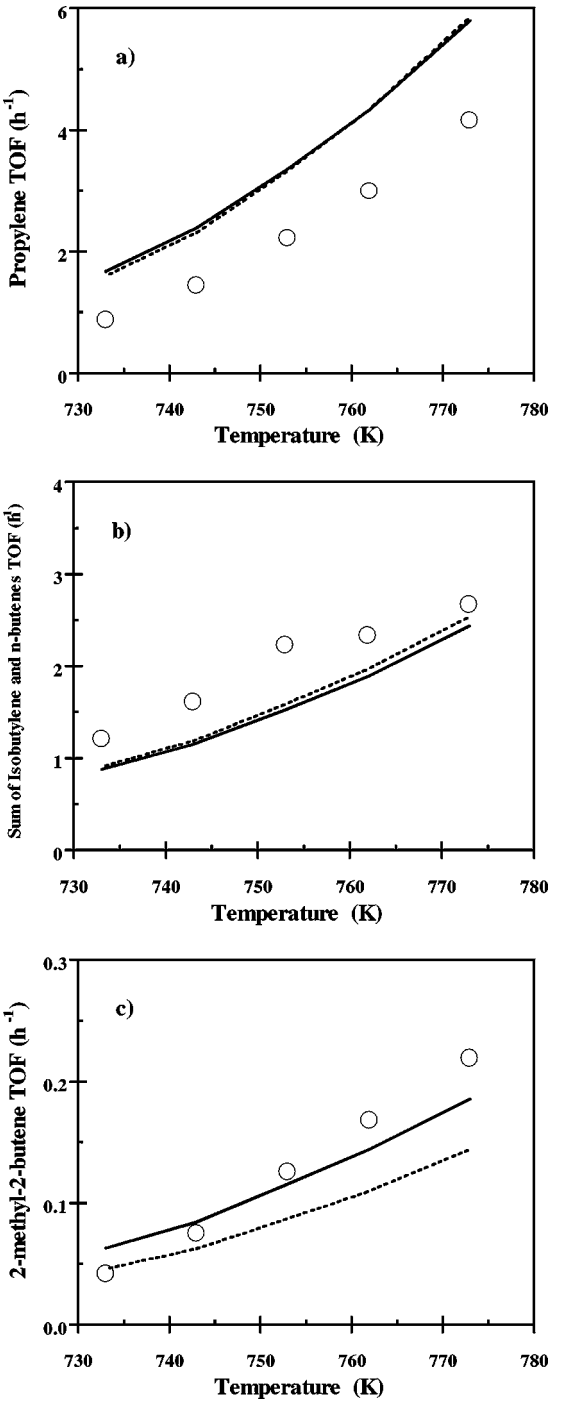

FIG. 10. (a) Propylene TOF, (b) sum of isobutylene and *n*-butenes TOF, and (c) 2-methyl-2-butene TOF, as a function of temperature for the data set at high temperature (42). The predictions of the kinetic model: solid line = full model; dotted line = simplified model.

Since we have multiple products, we summed the $X_{\mathrm{RC},i}$ over all products,

$$\sum |X_{\mathrm{RC},i}| = \sum_n \left| \left(\frac{\partial r_n}{\partial k_{i,\mathrm{for}}} \right)_{K_{\mathrm{eq},i,k_j}} \frac{k_{i,\mathrm{for}}}{r} \right| = \sum_n \left| \left(\frac{\partial r_n}{\partial k_{i,\mathrm{rev}}} \right)_{K_{\mathrm{eq},i,k_j}} \frac{k_{i,\mathrm{rev}}}{r} \right|, \qquad [13]$$

where r_n refers to the rate of production of species n. We use the absolute value in this sum since a given kinetic parameter may have a positive sensitivity for a given product and a negative sensitivity for another product.

Table 3 shows the steps with the highest degrees of rate control for representative points at low and high temperatures. The most sensitive steps involve hydride transfer of surface species with isobutane and oligomerization/β-scission steps involving primarily adsorbed C_8 and C_7 species. The two steps for isobutane activation are kinetically significant only under the high-temperature reaction conditions.

TABLE 3

Reaction Steps with Highest Degree of Rate Control ($\Sigma|X_{\mathrm{RC},i}|$)

Step	$\Sigma\lvert X_{RC,i}\rvert$	
	523 K	773 K
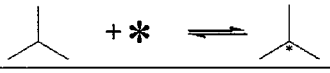	—	3.2
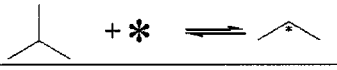	—	3.9
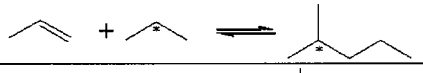	—	0.3
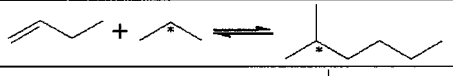	0.1	0.2
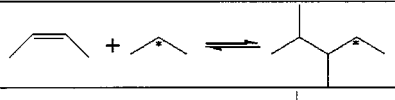	0.4	0.5
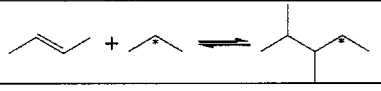	0.4	0.5
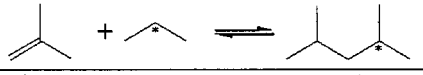	—	0.9
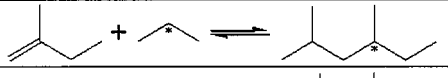	1.2	1.1
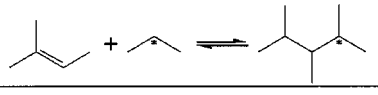	1.3	0.7
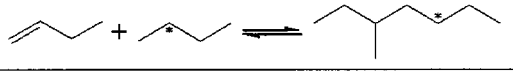	0.2	0.2
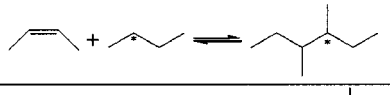	0.9	0.5
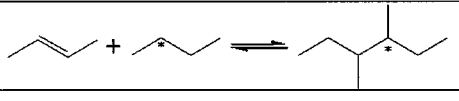	0.9	0.5
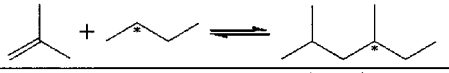	1.0	0.5
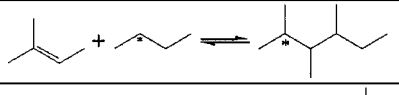	—	0.2
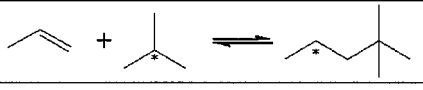	—	0.1

TABLE 3—*Continued*

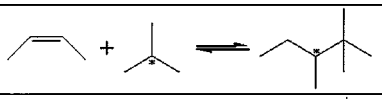	0.2	—
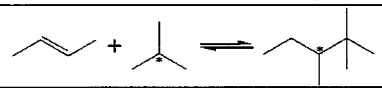	0.2	—
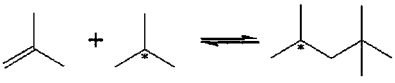	0.5	0.3
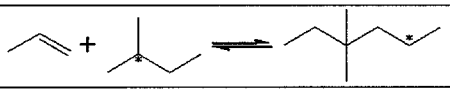	0.1	0.2
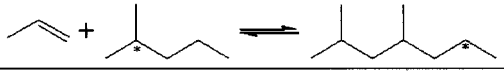	—	0.4
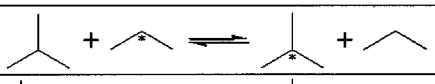	1.5	3.5
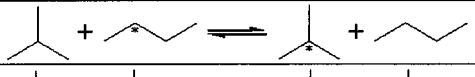	2.8	1.2
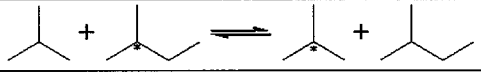	0.1	1.6
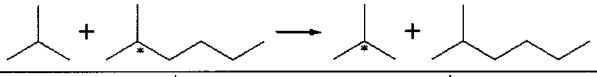	0.2	0.1
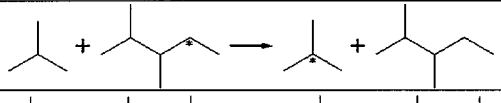	0.5	0.2
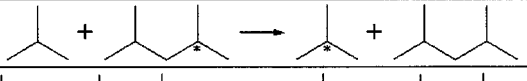	0.2	—
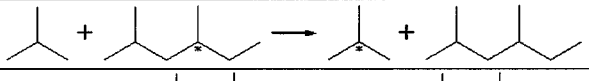	1.1	—
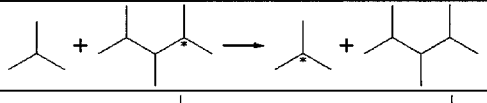	1.2	—
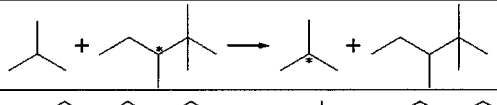	0.1	—
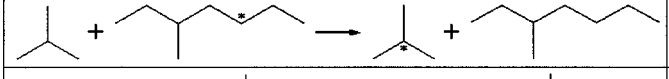	0.2	—
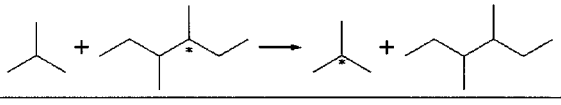	0.3	—

Simplified Kinetic Model

We generated a simplified reaction scheme based on the steps shown in Table 3 that were found to have the highest degrees of rate control for representative points at low and high temperatures. This simplified scheme, shown in Fig. 11, includes 2 protolysis steps, 7 adsorption/desorption steps (for the 7 olefins that are observed experimentally), 18 oligomerization/β-scission steps, 10 isomerization steps, and 11 hydride transfer steps. While the isomerization steps are not kinetically significant, they are required to convert between various isomers formed in different oligomerization/β-scission steps.

A simplified kinetic model may be constructed from the steps in Fig. 11, using the same values for kinetic parameters as determined from the full kinetic model. The results predicted by the simplified model are shown as dashed curves in Figs. 3–10. In general, the results obtained from the simplified reaction scheme are in approximate agreement with those obtained from the full model. For the reaction kinetics data obtained at the lower temperatures of the present study, the largest difference between the

No	Step
1	
2	
3	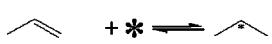
4	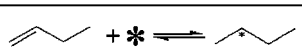
5	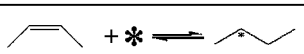
6	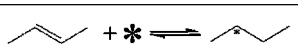
7	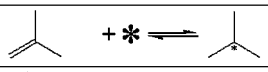
8	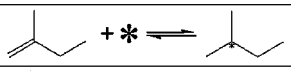
9	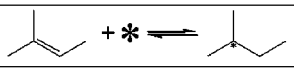
10	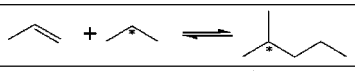
11	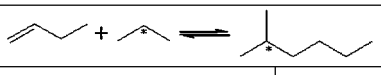
12	
13	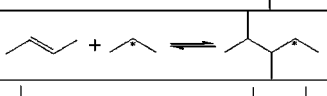
14	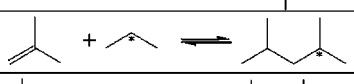
15	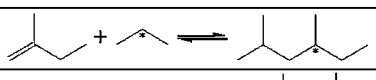
16	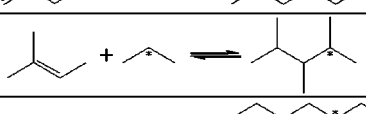
17	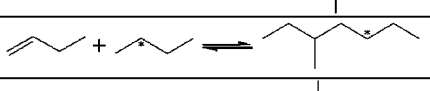
18	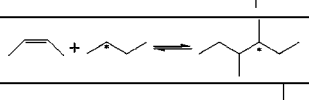
19	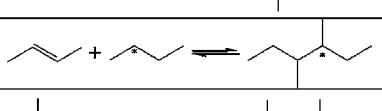
20	
21	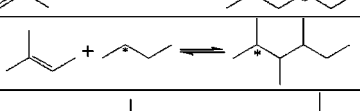
22	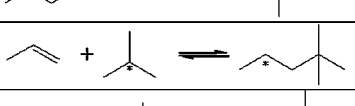
23	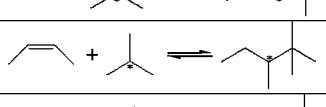
24	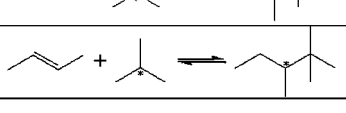

No	Step
25	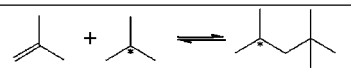
26	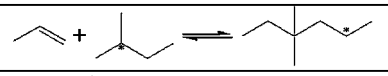
27	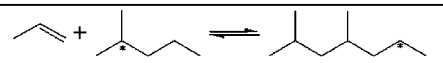
28	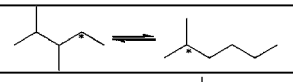
29	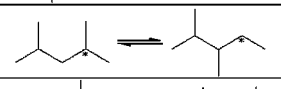
30	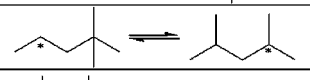
31	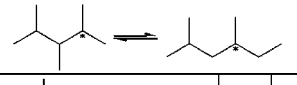
32	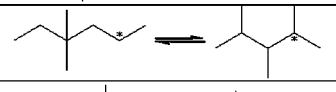
33	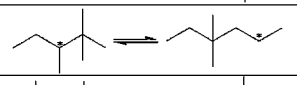
34	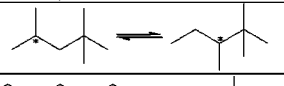
35	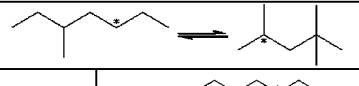
36	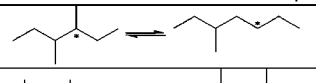
37	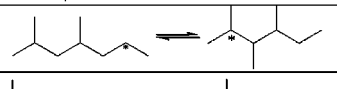
38	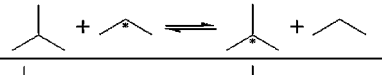
39	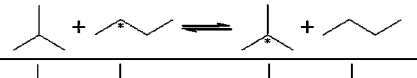
40	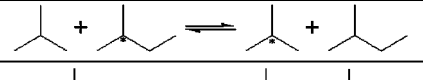
41	
42	
43	
44	
45	
46	
47	
48	

FIG. 11. Simplified reaction scheme for isobutane conversion on a USY zeolite catalyst.

predictions of both models was found for the experiments conducted at 523 K and 80% of isobutane in the feed. For the reaction kinetics data collected by Yaluris *et al.* (42) at higher temperatures, the largest differences in the predictions of both models were found for isopentane and 2-methyl-2-butylene. The agreement, in several cases, between the simplified and the full kinetic models confirms our conclusions, deduced from sensitivity analyses, about the nature of the significant steps in the full model.

CONCLUSIONS

Reaction kinetics studies were conducted at low temperatures (523–573 K), where the reaction is initiated by the addition of isobutylene (e.g., from 50 to 400 ppm) to the reactor feed. A kinetic model for isobutane conversion on USY zeolite over a wide range of reaction conditions is developed from the results of this study, combined with data from previous kinetics studies for isobutane conversion at higher temperatures (733–773 K), where the reaction is initiated by the activation of isobutane. According to our kinetic model, the rates of production of all reaction products can be described in terms of well-established chemistry, involving the following families of reactions: adsorption/desorption steps, oligomerization/β-scission processes, isomerization steps, hydride transfer processes, and initiation steps. The kinetic model is based on a limited number of kinetic parameters that describe the reactivity trends for different hydrocarbon species. The reactive intermediates on the acid sites are assumed to be neutral alkoxy species, and the strength of interaction of these species with the zeolite is assumed to be a linear function of the chain length. This kinetic model, based on initiation, propagation, and termination steps of a surface chain reaction scheme is able to bridge the kinetics of isobutane conversion at low and high temperatures by changing the nature of the initiation steps, while maintaining the same propagation and termination steps. Sensitivity analyses of the 370 steps of the full kinetic model indicate that reaction kinetics at low and high temperatures are controlled by the rates of 31 steps. A simplified kinetic model based on these sensitive steps is adequate to describe the experimental trends for isobutane conversion at temperatures from 523 to 773 K.

APPENDIX: GENERATION OF REACTION SCHEME

We outline below a procedure to generate the complete reaction scheme used in our kinetic model for isobutane conversion over USY zeolite.

1. Start with the following seven olefin species that are observed experimentally under our reaction conditions: propene, 1-butylene, *cis*-butylene, *trans*-butylene, isobutylene, 2-methyl-1-butylene, and 2-methyl-2-butylene.

2. Generate the corresponding four surface species:

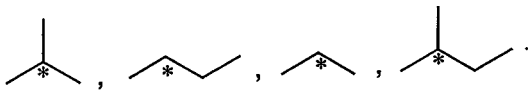

3. React each of the olefins given in part (1) with each of the surface species in part (2) according to Markovnikov's rule.

Note: This procedure leads to 28 reaction steps, which generate 1 C_6 species, 5 C_7 species, 8 C_8 species (the same C_8 species results from reactions of 2-methyl-1-butylene with adsorbed C_3 species and 1-butylene with adsorbed normal C_4 species), 7 C_9 species, and 2 C_{10} species.

4. React each of the species mentioned in part (3) with all of the olefins mentioned in part (1), except for the two C_5-olefins (since the concentration of C_5-olefins in the product stream is low). Do not include reactions that lead to the formation of species with more than 12 carbon atoms.

Note: This procedure leads to 77 steps (i.e., $(1)(5)+(5)(5)+(8)(5)+(7)(1)=77$). These steps generate 1 C_9 species, 8 C_{10} species, 20 C_{11} species, and 31 C_{12} species.

5. React the new C_9 species with propylene to form another C_{12} species.

Note: At this point in the procedure, 106 oligomerization/β-scission steps, 88 surface species, and 7 olefins have been generated.

6. Divide all the surface species into different sets according to the number of carbon atoms they possess.

7. For each such set of part (6), divide the species into subsets based on the number of branches they possess.

8. For species within the same subset of part (7), write isomerization steps that involve nonbranching rearrangements, so that each species in the subset can be directly or indirectly transformed to every other species in that subset.

9. Select one of the species from each of the subset of part (7), and write a branching rearrangement reaction between these species.

Note: Since the isomerization steps are quasi-equilibrated, it is not necessary to write all isomerization steps. Instead, it is sufficient to include steps whereby each species can be converted to each of the other species having the same number of carbon atoms, either directly or via a sequence of isomerization steps. In our reaction scheme, we introduced two new C_8 species to facilitate the branching rearrangements; these species were 2,3-dimethyl-hexyl and 2,3,3-trimethyl-pentyl-alkoxy species. As a result, 79 of such isomerization steps are required.

10. For each surface species, write steps that allow it to desorb as an olefin.

Note: This procedure leads to 94 adsorption/desorption steps, leading to 94 gaseous olefins. (Some surface species desorb to form different gaseous olefins.)

11. For each surface species (except isobutyl), write a step in which each undergoes hydride transfer with the isobutane to form the corresponding paraffin. Lump together all paraffins that have six or more carbon atoms ($C_{>5}$) into a single species, and assume that the hydride transfer reactions for $C_{>5}$ are irreversible.

Note: This procedure leads to 89 hydride transfer steps. The total number of paraffins should be five, including isobutane.

12. Write two steps representing the initiation processes at high temperature (i.e., isobutane protolysis), leading to two additional gaseous species: methane and hydrogen.

Note: At the end of the previously described procedures, the reaction scheme contains 2 protolysis steps, 94 adsorption/desorption steps, 106 oligomerization/β-scission steps, 79 isomerization steps, and 89 hydride transfer steps. Also, the reaction scheme contains 90 surface species, vacant sites, 94 gaseous olefins, 6 gaseous paraffins (including the lumped species), and gaseous hydrogen.

ACKNOWLEDGMENTS

We gratefully acknowledge the funding from the Department of Energy (Basic Energy Sciences) and Engelhard Corporation, which supported research at the University of Wisconsin. We wish to thank Dr. Xinsheng Liu at Engelhard who carried out the FTIR studies. We also extend our thanks to Christian Steinbeck and Jakob J. Krummenacher for their valuable assistance in the development of the experimental work.

REFERENCES

1. Corma, A., *Chem. Rev.* **95**, 559 (1995).
2. Martens, J. A., Souverijns, W., Van-Rhijn, W., and Jacobs, P. A., *in* "Handbook of Heterogeneous Catalysis" (G. Ertl, H. Knozinger, and J. Weitkamp, Eds.), Vol. 1, p. 324. VCH Verlagsgesellschaft mbH, Weinheim, 1997.
3. Lercher, J. A., Gruendling, C., and Eder-Mirth, G., *Catal. Today* **27**, 353 (1996).
4. Chen, D., Sharma, S., Cardona-Martinez, N., Dumesic, J. A., Bell, V., Hodge, G., and Madon, R. J., *J. Catal.* **136**, 392 (1992).
5. Eder, F., and Lercher, J. A., *Stud. Surf. Sci. Catal.* **97**, 495 (1995).
6. Gorte, R. J., and White, D., *Topics Catal.* **4**, 57 (1997).
7. Brunner, E., *Catal. Today* **38**, 361 (1997).
8. Eder, F., Stockenhuber, M., and Lercher, J. A., *J. Phys. Chem. B* **101**, 5414 (1997).
9. Gorte, R. J., and Biaglow, A. I., *Chem. Ind.* (*London*) **74**, 217 (1998).
10. Brait, A., Seshan, K., and Lercher, J. A., *Appl. Catal. A* **169**, 299 (1998).
11. Chakraborty, B., and Viswanathan, B., *Catal. Today* **49**, 253 (1999).
12. Hattori, H., Takahashi, O., Takagi, M., and Tanabe, K., *J. Catal.* **68**, 132 (1981).
13. Kramer, G. M., McVicker, G. B., and Ziemiak, J. J., *J. Catal.* **92**, 355 (1985).
14. Haag, W. O., Dessau, R. M., and Lago, R. M., *Stud. Surf. Sci. Catal.* **60**, 255 (1991).
15. Shigeishi, R., Garfoth, A., Harris, I., and Dwyer, J., *J. Catal.* **130**, 423 (1991).
16. Krannila, H., Haag, W. O., and Gates, B., *J. Catal.* **135** (1992).
17. Guisnet, M., Gnep, N. S., Aittaleb, D., and Doyomet, Y. J., *Appl. Catal. A* **87**, 255 (1992).
18. Zhao, Y., Bamwenda, G. R., Groten, W. A., and Wojciechowski, B. W., *J. Catal.* **140**, 243 (1993).
19. Asuquo, R. A., Eder-Mirth, G., and Lercher, J. A., *J. Catal.* **155**, 376 (1995).
20. Guisnet, M., and Gnep, N. S., *Appl. Catal. A* **146**, 33 (1996).
21. Narbeshuber, T. F., Brait, A., Seshan, K., and Lercher, J. A., *Appl. Catal. A* **146**, 119 (1996).
22. Narbeshuber, T. F., Stockenhuber, M., Brait, A., Seshan, K., and Lercher, J. A., *J. Catal.* **160**, 183 (1996).
23. Fogash, K. B., Larson, R. B., Gonzalez, M. R., Kobe, J. M., and Dumesic, J. A., *J. Catal.* **163**, 138 (1996).
24. Asuquo, R. A., Eder-Mirth, G., Seshan, K., Pieterse, A. A. Z., and Lercher, J. A., *J. Catal.* **168**, 292 (1997).
25. Babitz, S. M., Kuehne, M. A., and Kung, H. H., *Ind. Eng. Chem. Res.* **36**, 3027 (1997).
26. Yaluris, G., Madon, R. J., and Dumesic, J. A., *J. Catal.* **165**, 205 (1997).
27. Cortright, R., Dumesic, J. A., and Madon, R. J., *Topics Catal.* **4**, 15 (1997).
28. Brait, A., Koopmans, A., Weinstabl, H., Ecker, A., Seshan, K., and Lercher, J. A., *Ind. Eng. Chem. Res.* **37**, 873 (1998).
29. Tran, M. T., Gnep, N. S., Szabo, G., and Guisnet, M., *J. Catal.* **174**, 185 (1998).
30. Hong, Z., Fogash, K. B., Watwe, R. M., Kim, B., Masqueda-Jimenez, B. I., Natal-Santiago, M. A., Hill, J. M., and Dumesic, J. A., *J. Catal.* **178**, 489 (1998).
31. Babitz, S. M., Williams, B. A., Miller, J. T., Snurr, R. Q., Haag, W. O., and Kung, H. H., *Appl. Catal. A* **179**, 71 (1999).
32. Hong, Z., Fogash, K. B., and Dumesic, J. A., *Catal. Today* **51**, 269 (1999).
33. Williams, B. A., Babitz, S. M., Miller, J. T., Snurr, R. Q., and Kung, H. H., *Appl. Catal. A* **177**, 161 (1999).
34. Kung, H. H., Williams, B. A., Babitz, S. M., Miller, J. T., and Snurr, R. Q., *Catal. Today* **52**, 91 (1999).
35. McVicker, G. B., Kramer, G. M., and Ziemiak, J. J., *J. Catal.* **83**, 286 (1983).
36. Lombardo, E. A., and Hall, W. K., *J. Catal.* **112**, 565 (1988).
37. Engelhardt, J., and Hall, W. K., *J. Catal.* **125**, 472 (1990).
38. Stefanadis, C., Gates, B. C., and Haag, W. O., *J. Mol. Catal.* **67**, 363 (1991).
39. Shertukde, P. V., Marcelin, G., Sill, G. A., and Hall, W. K., *J. Catal.* **136**, 446 (1992).
40. Rekoske, J. E., Madon, R. J., Aparicio, L. M., and Dumesic, J. A., *Stud. Surf. Sci. Catal.* **75**, 1653 (1993).
41. Corma, A., Miguel, P. J., and Orchillés, A. V., *J. Catal.* **145**, 171 (1994).
42. Yaluris, G., Rekoske, J. E., Aparicio, L. M., Madon, R. J., and Dumesic, J. A., *J. Catal.* **153**, 54 (1995).
43. Yaluris, G., Rekoske, J. E., Aparicio, L. M., Madon, R. J., and Dumesic, J. A., *J. Catal.* **153**, 65 (1995).
44. Engelhardt, J., *J. Catal.* **164**, 449 (1996).
45. Fogash, K. B., Hong, Z., Kobe, J. M., and Dumesic, J. A., *Appl. Catal. A* **172**, 107 (1998).
46. Fogash, K. B., Hong, Z., and Dumesic, J. A., *J. Catal.* **173**, 519 (1998).
47. Engelhardt, J. and Valyon, J., *J. Catal.* **181**, 294 (1999).
48. Cortright, R. D., Fogash, K. B., and Dumesic, J. A., *J. Catal.* **181**, 299 (1999).
49. Liu, X., Truitt, R. E., and Hodge, G. D., *J. Catal.* **176**, 52 (1998).
50. Hilaireau, P., Bearez, C., Chevalier, F., Perot, G., and Guisnet, M., *Zeolites* **2**, 69 (1982).
51. Bearez, C., Chavalier, F., and Guisnet, M., *React. Kinet. Catal. Lett.* **22**, 405 (1983).
52. Liguras, D. K., and Allen, D. T., *Ind. Eng. Chem. Res.* **28**, 665 (1989).

53. Liguras, D. K., and Allen, D. T., *Ind. Eng. Chem. Res.* **28**, 674 (1989).
54. Quann, R. J., and Jaffe, S. B., *Ind. Eng. Chem. Res.* **31**, 2483 (1992).
55. Quann, R. J., and Jaffe, S. B., *Chem. Eng. Sci.* **51**, 1615 (1996).
56. Watson, B. A., Klein, M. T., and Harding, R. H., *Ind. Eng. Chem. Res.* **35**, 1506 (1996).
57. Watson, B. A., Klein, M. T., and Harding, R. H., *Ind. Eng. Chem. Res.* **36**, 2954 (1997).
58. Watson, B. A., Klein, M. T., and Harding, R. H., *Appl. Catal. A* **160**, 13 (1997).
59. Froment, G. F., *Catal. Today* **52**, 153 (1999).
60. Clymans, P. J., and Froment, G. F., *Comput. Chem. Eng.* **8**, 137 (1984).
61. Baltanas, M. A., and Froment, G. F., *Comput. Chem. Eng.* **9**, 71 (1985).
62. Feng, W., Vynckier, E., and Froment, G. F., *Ind. Eng. Chem. Res.* **32**, 2997 (1993).
63. Yaluris, G., Madon, R. J., and Dumesic, J. A., *J. Catal.* **186**, 134 (1999).
64. Kazansky, V. B., and Senchamya, I. N., *J. Catal.* **119**, 108 (1989).
65. Kazansky, V. B., Frash, M. V., and van-Santen, R. A., *Catal. Lett.* **48**, 61 (1997).
66. Frash, M. V., and van-Santen, R. A., *Topics Catal.* **9**, 191 (1999).
67. Natal-Santiago, M. A., Alcala, R., and Dumesic, J. A., *J. Catal.* **181**, 124 (1999).
68. Haag, W. O., *in* "Zeolites and Related Microporous Materials: State of the Art 1994" (J. Weitkamp, H. G. Karge, H. Pfeifer, and W. Holderich, Eds.), Vol. 84, p. 1375. Elsevier Science, Amsterdam, 1994.
69. Eder, F., and Lercher, J. A., *Zeolites* **18**, 75 (1997).
70. Denayer, J. F., Baron, G., Martens, J., and Jacobs, P., *J. Phys. Chem. B* **102**, 3077 (1998).
71. van-Well, W. J. M., Janchem, J., de-Haan, J. W., and van-Santen, R. A., *J. Phys. Chem. B* **103**, 1841 (1999).
72. Williams, B. A., Ji, W., Miller, J. T., Snurr, R. Q., and Kung, H. H., *Appl. Catal.* **203**, 179 (2000).
73. Martens, G. G., Marin, G. B., Martens, J. A., Jacobs, P. A., and Baron, G. V., *J. Catal.* **195**, 253 (2000).
74. Benson, S. W., "Thermochemical Kinetics." Wiley, New York, 1968.
75. Benson, S. W., and Buss, J. H., *J. Chem. Phys.* **29**, 546 (1969).
76. Benson, S. W., Cruickshank, F. R., Golden, D. M., Haugen, G. R., O'Neal, H. E., Rodgers, A. S., Shaw, R., and Walsh, R., *Chem. Rev.* **69**, 279 (1969).
77. Reid, R. C., Prausnitz, J. M., and Poling, B. E., "The Properties of Gases and Liquids." McGraw–Hill, New York, 1987.
78. Kazansky, V. B., Frash, M. V., and van-Santen, R. A., *Appl. Catal. A* **146**, 225 (1996).
79. Rigby, A. M., Kramer, G. J., and van-Santen, R. A., *J. Catal.* **170**, 1 (1997).
80. van-de-Runstraat, A., van Grondelle, J., and van-Santen, R. A., *Ind. Eng. Chem. Res.* **36**, 3116 (1997).
81. van-Santen, R. A., *Catal. Today* **50**, 511 (1999).
82. Boudart, M., "Kinetics of Chemical Processes." Butterworth-Heinemann, London, 1991.
83. Stewart, W. E., and Caracotsios, M. C., "Athena Visual Workbench." Stewart & Associates Engineering Software, Madison, WI 2000.
84. Campbell, C. T., *Topics Catal.* **1**, 353 (1994).